Non-resolved detection of objects performing On Orbit Servicing in Geostationary orbit

Robert (Lauchie) Scott
Defence R&D Canada – Ottawa, PhD Candidate, Carleton University, Ottawa, Ontario
Dr. Alex Ellery
Department of Mechanical and Aerospace Engineering, Carleton University, Ottawa, Ontario
Dr. Martin Levesque
Defence R&D Canada – Valcartier

Abstract

On Orbit Servicing (OOS) of geostationary (GEO) satellites represents a new robotic space mission paradigm which could extend the life of existing satellites and reduce the rate of space debris generation. This mission type poses unique challenges for traditional optical space surveillance sensors. As the satellites perform close proximity operations, a distant observer sees the two objects as a single point source on a CCD (Charged Couple Device) as the objects' angular separations, as viewed from a distant observer, are much smaller than the point source size of a typical space surveillance instrument. This analysis explores the unforced relative motion flight of a servicer satellite about its client GEO satellite with separations of 100 meters or less. Tools developed to address the physical and optical reflectance characteristics of this kind of mission type along with example light curves for diffuse optical reflections from both satellites performing OOS are presented. These tools create synthetic light curve data to permit future testing of light curve inversion and signal separation as a means to infer the relative motion of a secondary object about a GEO satellite.

1. Introduction

On Orbit Servicing (OOS) is a broad subject area and the types of orbital operations performed by this class of space mission include: on-orbit satellite inspection, rendezvous, docking, repair, consumables replenishment, technology refresh, orbital modification or orbital construction. OOS has been demonstrated in the manned space realm on Skylab, Westar, Palapa-B2, Solar Max, Hubble and the International Space Station servicing missions [1].

In recent years the technologies for autonomous robotic satellites to perform OOS in Earth orbit have matured considerably. OOS demonstration missions such as Orbital Express [2][3], and various related rendezvous and robotics technology demonstration missions [4][5] have been flown. Refueling of geostationary satellites with station keeping propellant is an appealing mission possibility due to the high expense of satellite replacement in GEO since GEO satellite lifetime is generally limited by the amount of fuel consumed. The European Space Agency studied the economic and technical [6] viability of GEO satellite orbital refueling but did not fly demonstrators. Commercial entities are also reexamining robotic geostationary satellite refueling [7][8]. While satellite refueling is the primary rationale for OOS, satellite inspection and repair, such as the freeing of undeployed solar arrays or antenna reflectors, shows promise with the proposed space robotic manipulator technology.

This new mission class poses issues for the space situational awareness (SSA) community. Many of the optical deep-space SSA sensors perform metric tracking using angles-only measurements to update the orbital catalog. OOS poses issues for such sensors as the satellites are performing relative flight in very close proximity to one another and the observed object pair would appear combined as a single point source on a focal-plane array (typically CCD) detector. Traditional detection approaches such as pixel clustering are unable to resolve and differentiate the two individual objects. If a secondary ("servicer") satellite can approach and rendezvous with a primary ("client") satellite, unnoticed by SSA sensors, this could be viewed as threat to the client spacecraft. The obvious indicator of another satellite's presence close to a client GEO would be an increase in brightness or radar cross section, but various sized servicers may not produce obvious indications of their presence. Another issue is one of orbital safety. If an object is suspected to be in close formation flight about a satellite it is difficult to obtain knowledge of the relative motion and separation between them. While large optical systems are better positioned to take high resolution imagery of objects and possibly resolve them as individual entities, small and low cost optical systems would have issues attempting to gain insight into the relative motion of the objects.

The majority of the proposed servicer concepts assume the use of an optical tracking sensor on the servicer satellite as the primary means to reckon relative position and orientation between the client and servicer. This analysis assumes that these cameras are fixed to the body frame of the servicer satellite, enforcing an attitude constraint on one of the axis of the servicer satellite to maintain the client in the field of view of the camera. It is postulated that the relative attitude motion of the servicer acts as a modulation source of the reflected sunlight as seen by the observer. The servicer's camera axis is constrained toward the client during its relative motion flight. The relative motion of the client and the servicer creates a time varying attitude profile by which the servicer must slew toward the client to maintain its situational awareness of the client.

To model the dynamics of this problem, both relative motion and optical reflectance simulations need to be developed. These tools will then be used to explore light curve inversion and signal separation to infer the presence and relative motion of the secondary satellite. This paper concludes with example light curves from diffuse reflection conditions for objects undergoing co-elliptic drift (linear) motion with the GEO client and elliptic (football) motions about the client.

The scope of this study is limited to the cases where the client and servicer are in unforced (non-propulsive) relative motion flight with one another, and are separated by less than one arcsecond (~200 meters) as observed from the ground. For cases where the satellites are separated by several kilometers or more, it is assumed that SSA sensors will detect the secondary satellite as a separate uncorrelated track during routine catalog maintenance. Also, this analysis also does not examine the case where a servicer is hard docked with its client.

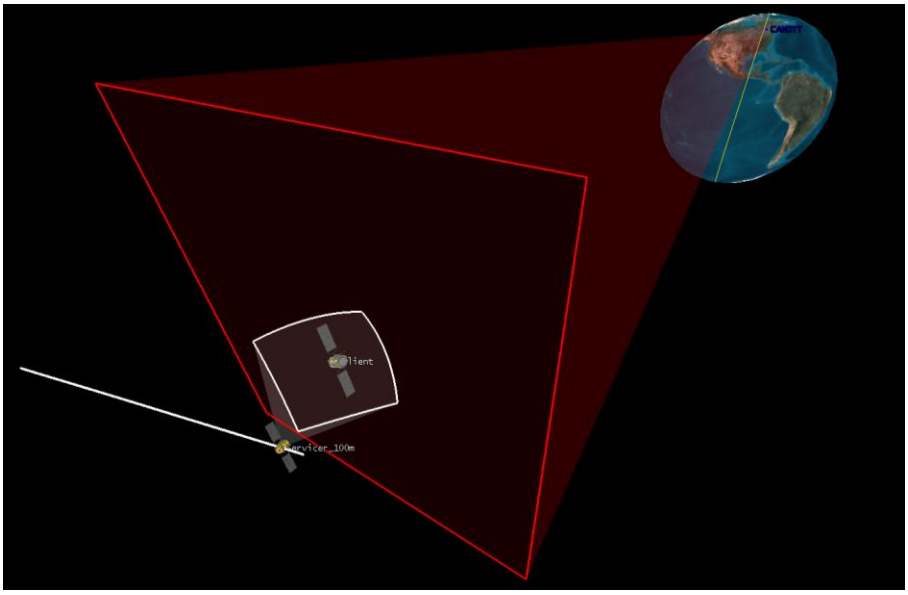

Fig. 1. Angular extent of a 1x1 arcsecond CCD pixel on OOS proximity operations in GEO (red). The relative motion between client and servicer occurs at scales much smaller than the resolving power of the observing sensor.

2. Modeling OOS

In this paper, the client satellite is defined to be the satellite to which the "service" (refueling or inspection service) is being supplied. The servicer is the satellite which is performing the robotic intervention and "works" on the client. The client is considered to be an operational (three axis stabilized) geostationary satellite which has its bus fixed toward nadir (Earthward). The servicer is attitude constrained such that its tools (camera, robotics, etc) are pointed toward its "work" (the client satellite).

To model relative motion flight, the Hill frame of motion [9] is well suited for the analysis of the client and servicer pair. The Hill equations of motion are often used to describe the dynamics of satellites in relative motion where the client moves in a circular orbit. These relationships (see equation 1) work well to first order for short time spans in GEO orbit since lunisolar orbital perturbations, solar radiation pressure and longitudinal gravitational accelerations

act similarly on both objects and can be neglected. The coordinate frame is also convenient as the client is fixed in this frame, pointing Earthward. The servicer is assumed to follow unforced relative motion trajectories where no propulsive action is taking place. The Hill coordinate frame is centered on the client satellite and $[x(t), y(t), z(t)]^T$ is the radial, intrack and crosstrack position vector of the of the servicer while $[x_0, y_0, z_0]^T$ are the initial position and velocity conditions of the servicer's relative motion. ω is the mean motion of the client satellite's orbit and is equivalent to the sidereal rotation rate of the Earth (7.29 x 10^{-5} rad/sec). These equations are coupled in the radial and intrack directions, while the z direction is uncoupled.

$$\begin{bmatrix} x(t) \\ y(t) \\ z(t) \\ \dot{x}(t) \\ \dot{y}(t) \\ \dot{z}(t) \end{bmatrix} = \begin{bmatrix} 4-3\cos(\omega t) & 0 & 0 & \frac{1}{\omega}\sin(\omega t) & \frac{2}{\omega}(1-\cos(\omega t)) & 0 \\ 6(1-\cos(\omega t)) & 1 & 0 & \frac{2}{\omega}(\cos(\omega t)-1) & \frac{4}{\omega}(\sin(\omega t)-3t) & 0 \\ 0 & 0 & \cos(\omega t) & 0 & 0 & \frac{1}{\omega}\sin(\omega t) \\ 3\omega\sin(\omega t) & 0 & 0 & \cos(\omega t) & 2\sin(\omega t) & 0 \\ 6\omega(\cos(\omega t)-1) & 0 & 0 & -2\sin(\omega t) & 4\cos(\omega t)-3 & 0 \\ 0 & 0 & -\omega Sin(\omega t) & 0 & 0 & \cos(\omega t) \end{bmatrix} \begin{bmatrix} x_0 \\ y_0 \\ z_0 \\ \dot{x}_0 \\ \dot{y}_0 \\ \dot{z}_0 \end{bmatrix} \quad (1)$$

Two special cases of relative motion are examined in this paper as general relative Hill motion has a large variable space to analyze. The co-elliptic drift orbit (linear motion with respect to the client) and Clohessy Wiltshire football (CW Football) resulting in elliptic motion are examined. Figure 2 shows examples of these kinds of relative motion and the initial conditions that the servicer needs to have relative to the client for these types of motion to occur. Elliptic safety ellipses have been proposed [1] for OOS missions in GEO to prevent the orbital velocity vectors from crossing one another and are manifested as a small inclination shift relative to the client; the safety ellipse is not presented here but will be analyzed in the future.

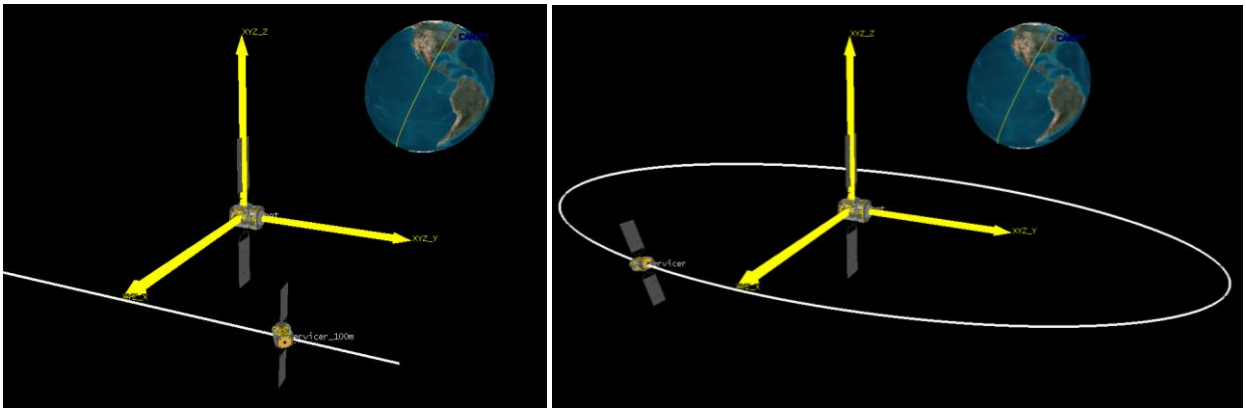

Fig. 2. (Left) Co-elliptic drift motion resulting in linear motion with respect to the client satellite with initial condition of $\dot{y}_0 = -\frac{3}{2}x_0\omega$. (Right) Elliptic motion of the servicer about the client resulting from the initial condition of $\dot{y}_0 = -2\omega x_0$

3. Light Curve Generation

Triangular polygon CAD models of satellites were created in ACAD3D™ and imported into Matlab™. Relative motion of the two objects were generated in Satellite Tool Kit™ and loaded as ephemeris data into the model. Material reflective properties are assigned to each facet using sample bidirectional reflectance distribution function (BRDF) models from [10] which captures specular and diffuse reflective properties of the satellite materials. At this time, the model does not account for object self-obscuration (satellite parts covering other satellite parts) and satellite self-shadowing of sunlight. This reflectance model also uses a BRDF adhering to a cosine lobe approximation where the peak reflected sunlight is aligned with the reflection vector $\mathbf{u_s}$ relative to the facet normal

and incident sunlight vectors (figure 3). Diffusely reflecting materials are modeled by assigning constant BRDF data to the satellite surface under study.

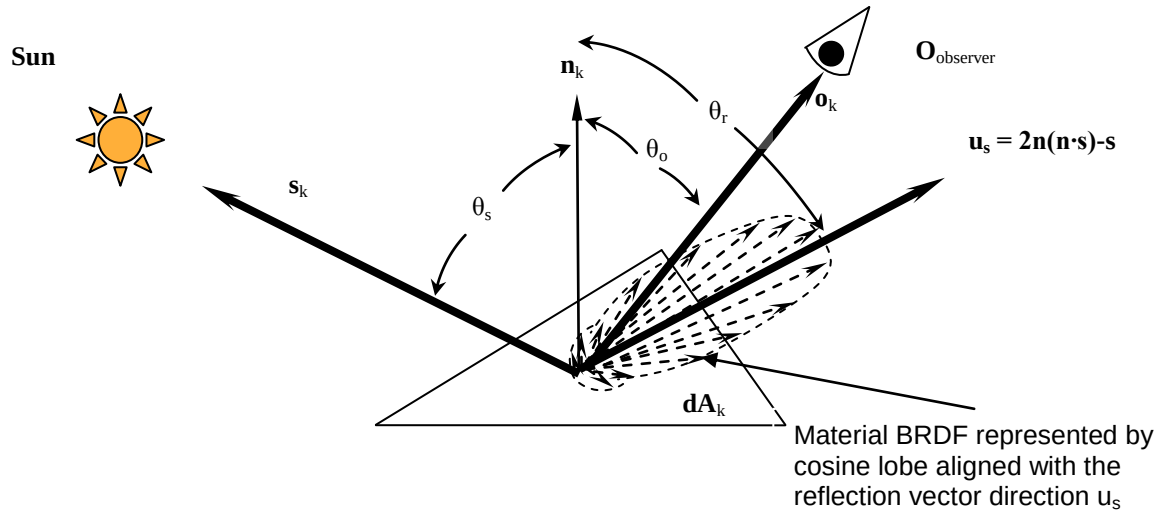

Fig. 3. Single polygon surface facet model of reflected sunlight.

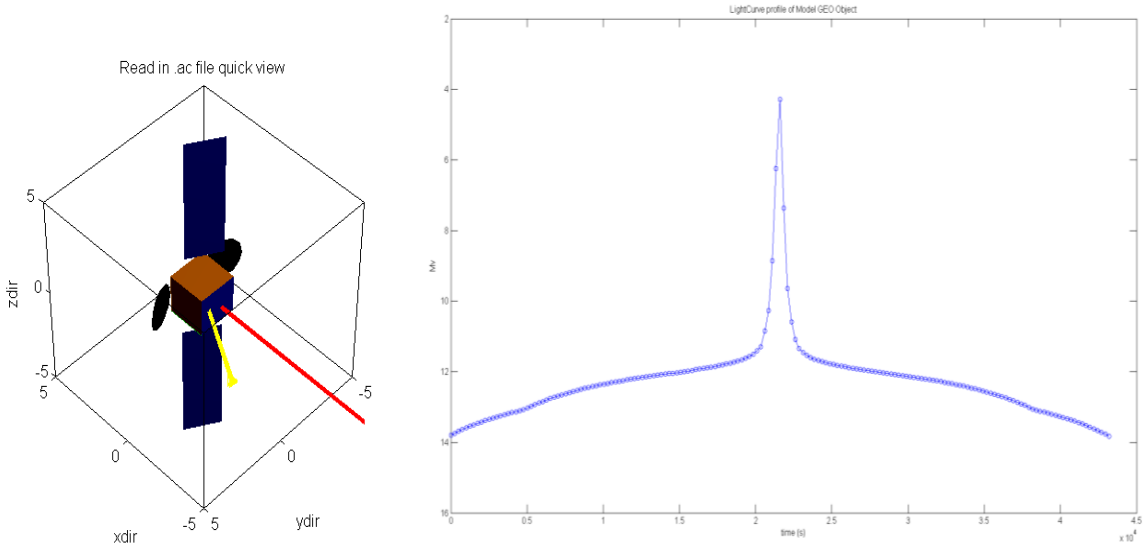

Fig. 4. Loaded CAD satellite (left) showing the sun vector (yellow) and observer vector (red). The resulting synthetic light curve showing solar panel glint at minimum phase (right)

4. Synthetic Light Curve Model and Assumptions

This analysis assumes that the servicer satellite is undergoing unforced relative motion profiles not exceeding distances larger than 100 meters from the client satellite. Further, this analysis also assumes that the client is a simplified object with diffusely reflecting sides and is a cubic, 3-axis stabilized bus with no outboard solar panel arrays. Future refinements will incorporate sun-pointed solar panel arrays aligned with the sun and realistic BRDFs for spacecraft material surfaces. The servicer is assumed to be of somewhat similar size and configuration to the client with the exception that one face of the servicer is constrained to point toward the client. The servicer's motion is assumed to be in the same plane (identical orbital inclination) with the client satellite. Assuming the solar flux

(F_{sun}) is constant (1380 W/m^2) over the observation time span, the sunlight reflected from the satellite bus toward the observer is the combination of light reflected from the summation of facets [11] from both the client and servicer satellites:

$$F_{total}(t) = \left(\frac{F_{sun}}{\pi} \sum_i aA_i \langle \mathbf{n}_i \cdot \mathbf{o} \rangle \langle \mathbf{n}_i \cdot \mathbf{s} \rangle \right)_{client} + \left(\frac{F_{sun}}{\pi} \sum_j aA_j \langle \mathbf{n}_j \cdot \mathbf{o} \rangle \langle \mathbf{n}_j \cdot \mathbf{s} \rangle \right)_{servicer} \quad (2)$$

where < > denotes the non-negative operator, **s**, **o**, **n** are the sun, observer and normal vectors in the body frame of the facets, *a* is the diffuse albedo of the surface, and *A* is the triangular surface area of the facets (denoted by indices *i* and *j*) as defined in [11]. The sun and observer vectors are transformed to the Hill frame by use of the radial, intrack and cross track cross product transformations (R_{Hill}) from [9].

The time span of interest is defined by the GEO satellite's motion toward (and past) the antisolar direction relative to the Earth-Sun line. This is the ~12 hours of observation time that a ground-based visible light telescope could use during equinox conditions. As the client satellite is assumed to be fixed in the Hill frame a ground based observer would observe the same facet normal throughout the observation period. The brightness of the client would be modulated by the motion of the sun vector over (primarily) the nadir facet visible to the observer (as gimbaled solar panel contributions are ignored here). This causes the $\langle \mathbf{n}_i \cdot \mathbf{o} \rangle$ term to be approximately unity and is assigned as such here. The brightness of the client is modulated by the motion of sun vector over the nadir face of the client therefore is proportional to $\cos(\omega_e t - \varphi)$ where ω_e is the sidereal rotation rate of the earth and φ is an arbitrary offset (equation 4).

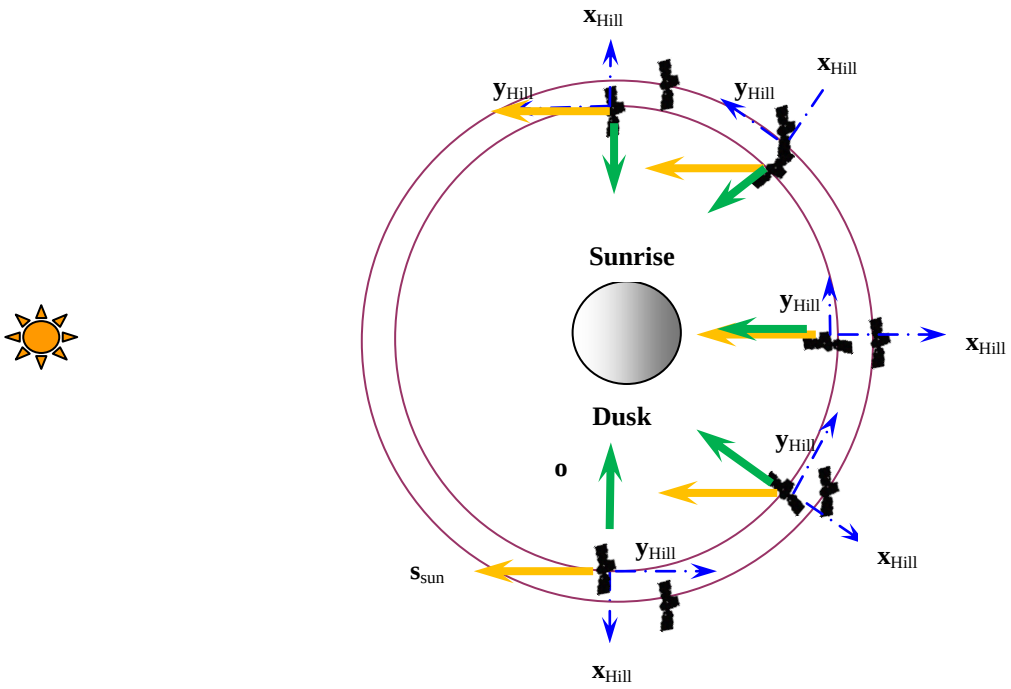

Fig. 5. Hill frame for analysis. The analysis time period begins at dusk (bottom) and rotates toward sunrise (top). The client and servicer are in a slightly different circular orbits during their relative motion flight

$$F_{client}(t) \approx \frac{F_{sun}}{\pi} aA \langle \mathbf{n} \cdot R_{Hill} \mathbf{s} \rangle \quad \text{or} \quad F_{client}(t) \approx \frac{F_{sun}}{\pi} aA \cos(\omega_e t - \phi) \quad (3,4)$$

The servicer's body normal vectors are rotated with respect to the Hill frame to track the client satellite by forcing its +x axis toward it (see figure 6). It should be noted that the observer and sun vectors are also assumed to be identical and the small offsets between the client and servicers sun and observer vectors are neglected.

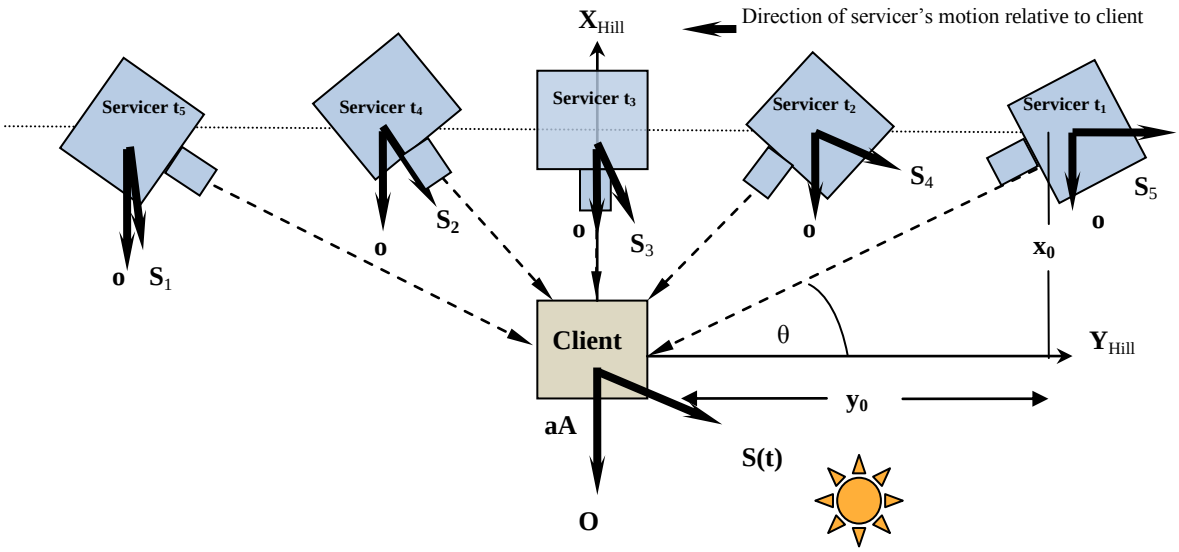

Fig. 6. Relative motion of servicer showing its slewing attitude motion with respect to the client (co-elliptic drift)

Since the servicer is attitude constrained it reorients its bus facet normals during relative motion with the client. For the case of co-elliptic drift (linear motion), the rotation angle and rotation matrix of the servicer about the Z direction (within the Hill frame) is expressed with respect to the initial conditions as equation 5 and 6.

$$\tan(\theta) = \frac{x_0}{y_0 - \frac{3}{2} x_0 \omega_e t} \qquad R_z(\theta) = \begin{bmatrix} \cos(\theta) & -\sin(\theta) & 0 \\ \sin(\theta) & \cos(\theta) & 0 \\ 0 & 0 & 1 \end{bmatrix} \tag{5,6}$$

θ is defined to be positive when the servicer is above the client in the radial direction and negative when the servicer is below. The R_z rotation (equation 6) is further complemented by an additional 90 degrees to align the +x axis of the servicer with that of the client.

For the case of elliptic motion where the client is located at the center of the ellipse, the servicer's attitude constraint rotation is described as equation 7.

$$\tan(\theta) = \frac{x_0 \cos(\omega t)}{-2 x_0 \sin(\omega t)} \tag{7}$$

The combined system's reflective contribution contains the servicer's rotational motion within the Hill reference frame in addition to the client's smooth cosine signal content.

$$F_{total}(t) = \frac{F_{sun}}{\pi} a A_c \cos(\omega_e t + \phi) + \frac{F_{sun}}{\pi} a A_S \sum_j \left\langle R_z(t)\mathbf{n}_j \cdot R_{Hill}\mathbf{o} \right\rangle \left\langle R_z(t)\mathbf{n}_j \cdot R_{Hill}\mathbf{s} \right\rangle \tag{8}$$

Light curve inversion requires the albedo-area terms to remain within the summation and use techniques identified in [11] to determine information on their content and constrain attitude. To continue this analysis, the coefficients of albedo-area and solar flux products become lumped constant parameters as K_1 and K_2 as the reflectivity and surface areas of the facets are identical in this case.

$$F_{total}(t) = K_1 \cos(\omega_e t + \phi) + K_2 \sum_j \left\langle R_z(t)\mathbf{n}_j \cdot R_{Hill}\mathbf{o} \right\rangle \left\langle R_z(t)\mathbf{n}_j \cdot R_{Hill}\mathbf{s} \right\rangle \tag{9}$$

This analysis will now look into the signal domain to analyze the periodic content of the modulated signal of the servicer with the client. It is further assumed that the observation and illumination vectors are in the plane of motion of the client-servicer pair. The rotation matrix, sun and observer vector are replaced by polar forms and complex conjugates are used to replace the dot product operations. As the observer vector is fixed in the Hill frame, no rotation is imposed. The sun vector is assumed to be constant over the time span of interest.

$$F_{total}(t) \approx K_1 e^{i(\omega_e t + \phi)} + K_2 \sum_j \left\langle e^{i(\theta(t)+\frac{\pi}{2})} e^{in_j} \cdot e^{i\psi_O} \right\rangle \left\langle e^{i(\theta(t)+\frac{\pi}{2})} e^{in_j} \cdot e^{i\omega_e t} e^{i\psi_s} \right\rangle \tag{10}$$

$$F_{total}(t) \approx K_1 e^{i\omega_e t + \phi} + K_2 \sum_j \left\langle e^{i(\theta(t)+\frac{\pi}{2})} e^{in_j} e^{i\psi_O} \right\rangle \left\langle e^{i(\theta(t)+\frac{\pi}{2})} e^{in_j} e^{i(\psi_s - \omega_e t)} \right\rangle \tag{11}$$

The contributions from the illuminated portions of the body are considered and the non-negative bracket operators are dropped.

$$F_{total}(t) \approx K_1 e^{i\omega_e t} + K_2 \sum_j e^{i(2\theta(t)+\pi)+2n_j+\psi_o+\psi_s-\omega_e t)} \tag{12}$$

$$F_{total}(t) \approx K_1 e^{i\omega_e t} + K_2 e^{iC+i(2\theta(t)-\omega_e t)} \tag{13}$$

In equation 13, *C* encapsulates amplitude and phase offset content due to the sun and observer vectors and θ indicates the relative rotation content. $\Omega_{mod,serv}$ is the time varying phase content of the measured signal.

$$\Omega_{\mathrm{mod},serv} = 2\theta(t) - \omega_e t \text{ or } \quad \frac{\Omega_{\mathrm{mod},serv} + \omega_e t}{2} = \theta(t) \tag{14}$$

A difficulty with this analysis is that it is not well suited for Fourier techniques as the measured signals comprise samples which are half period cosines (refer to figure 8 for examples). The signal content is also non-stationary and consists of discontinuities due to the sun vector illuminating new facets over the sharp edge of prismatic bodies (cusps in the left column of figure 8). These complications suggest wavelet analysis is better suited to identify local signal content within the light curves of these combined sources; such an analysis is beyond the scope of this work.

5. Synthetic Light Curves of Relative Motion

Two example light curve profiles are now presented. The first case is co-elliptic motion where the servicer satellite is in linear motion moving parallel to and toward the client satellite from above and later drifts past the client. The second case is a Clohessy Wiltshire football (elliptical motion) case. Both profiles are assumed to be near zero relative inclination with one another. Four offset distances (10, 25, 50 and 100 meters see figure 9) were simulated for the radial (x-offset) for the servicer relative to the client.

Features in figure 8 show that as the servicer's +x face moves relative to the client the light curves merge at minimum phase and the flux plots are correlated at minimum phase. This makes physical sense as the +x surface would be collinear with the nadir face of the client, resulting in similar reflectance behavior. The cusps visible in figure 8 are due to the sun vector transitioning between sharp edges on the facets of the servicer. The relative phase differences between the client and servicer light curve contributions may be separable in the frequency-phase domain. As the offset distance between the client and servicer becomes less (essentially the objects are in the same orbit) the light curves coalesce toward that of a single diffuse object signature (figure 8 bottom) This is due to the rate of relative motion decreasing significantly hence the slewing of the servicer becomes nearly negligible. This poses issues for analysis of objects which perform very close proximity flybys as the light curve may be indistinguishable from the servicer's contribution.

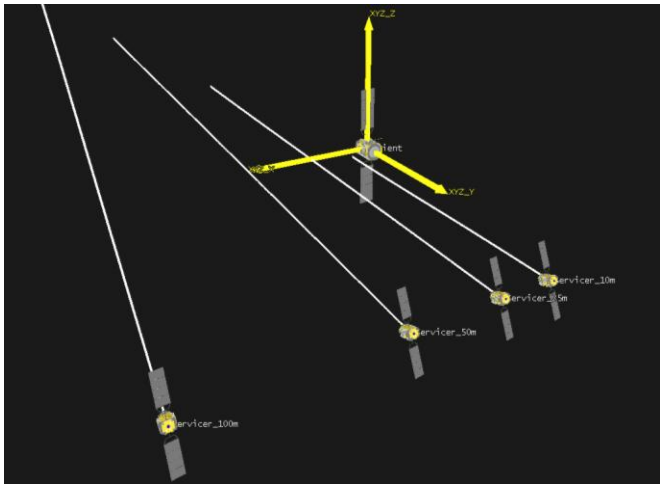

Fig. 7. Radially offset co-elliptic transfer relative motion test cases

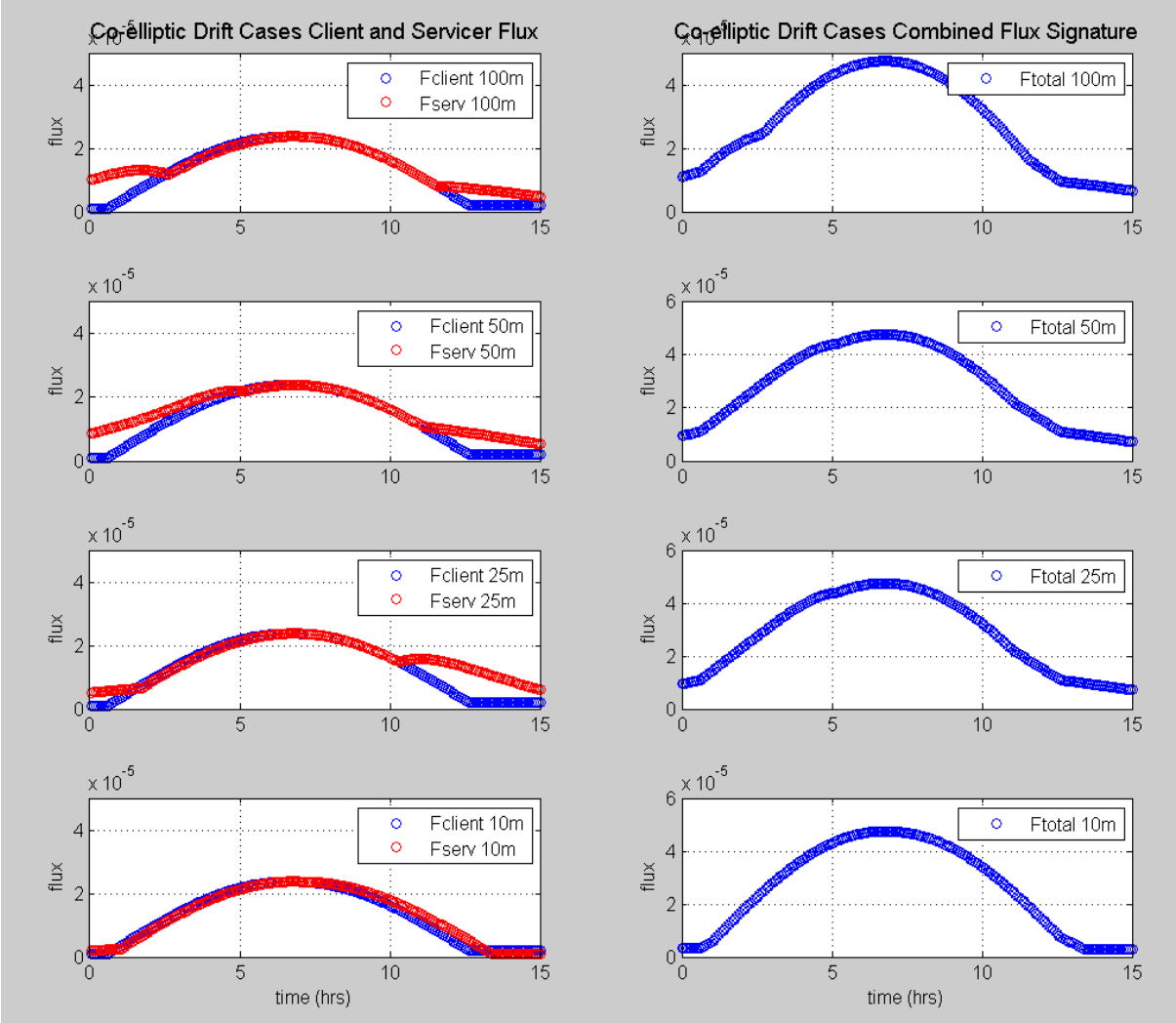

Fig. 8.(Left) Co-elliptic drift flux plots for 100m, 50m, 25m, 10m radial offsets between client (blue) and servicer red). (Right) Synthetic observed flux from combined object pair.

For the Hill "football" elliptic motion with the same radial offset conditions (see figure 9), the light curves are identical for all four test cases. All satellites complete their elliptic motion in one period and is non-Keplerian in nature. The attitude orientation of the servicer satellites maintains the same orientation and thus generates identical light curves. A possible marker that this type of motion is occurring is the skewness of the cosine curve which is due to the servicer's variable rate attitude motion (due to the quasi oscillatory nature of equation 7) to track the client.

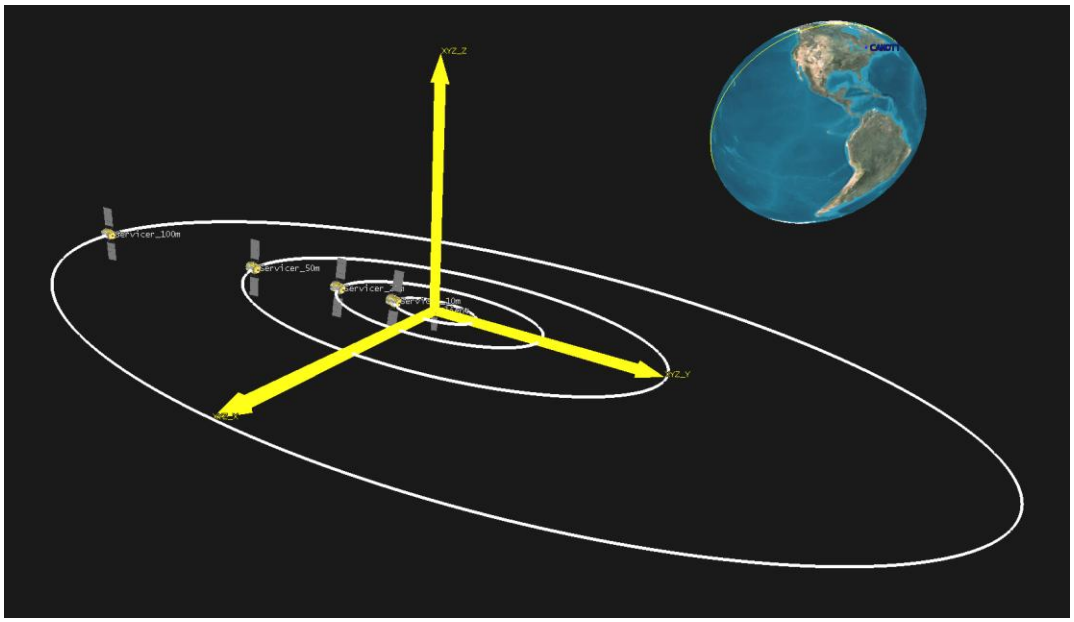

Fig. 9. CW Football (elliptic) motion of the servicer satellites about the client offset radially by 100, 50, 25 and 10m

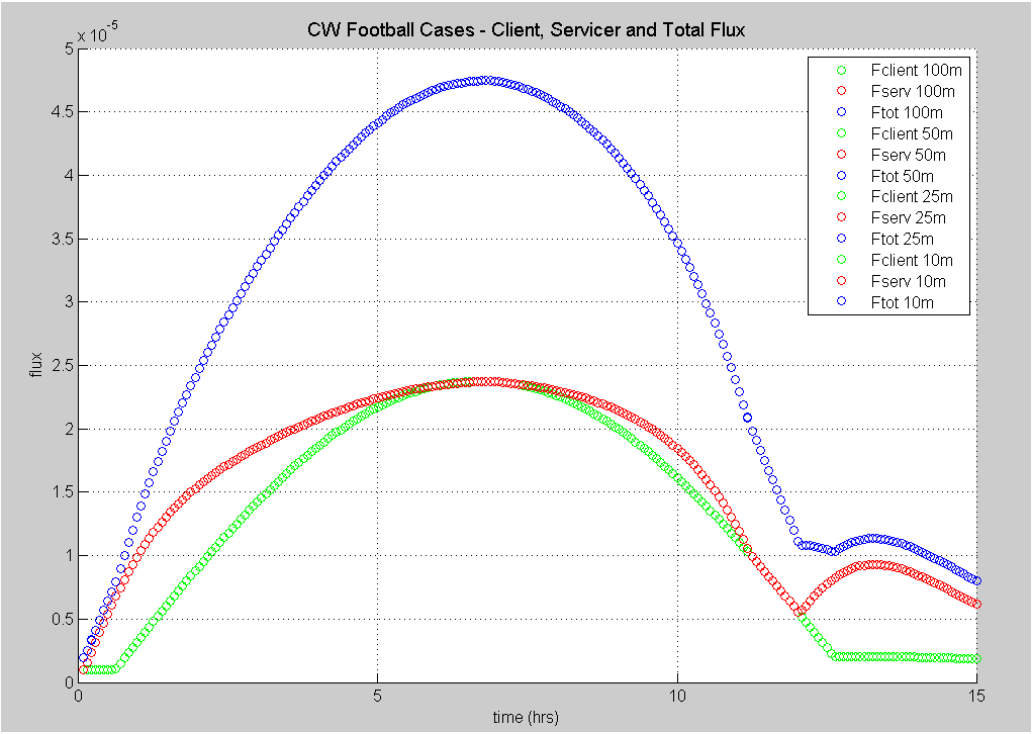

Fig. 10. Combined flux plots (blue) for the CW Football test cases For client (green) and servicer (red).

6. Conclusion and Future Analysis

Currently, the diffuse body reflection model of objects performing OOS in GEO suggests that the servicer's attitude motion may be observable as phase shift information content in optical light curves. To explore this possibility more fully, phase and frequency analysis will be performed on the simulated half period cosine response curves. Analysis of the cusp artifacts will also be employed to determine if the event when the sun vector transitions from one facet to another is another means to constrain object orientation. More analysis of the CW Football motion is needed in order to find a way to differentiate the relative radial offsets as their identical attitude rotation relative to the client makes it difficult to differentiate them.

Future work will also inspect the relative size issue where a small servicer is making an approach toward a large client. Specifically, the amount of light curve modulation that a small object causes on a large GEO satellite's light will be quantified. Blind source separation is another possible avenue to infer information about the client if other constraint characteristics about the mixing process of the light curves can be made. Enhancements to the reflection geometry incorporating more realistic BRDF models to capture specular phenomena will also be used to model the specular behavior of these objects.

7. References

1 NASA On Orbit Servicing Study Project Report. http://ssco.gsfc.nasa.gov/images/NASA_Satellite%20Servicing_Project_Report_0511.pdf Accessed 15 Jun 2011.

2 Mulder. T, "Orbital Express Autonomous Rendezvous and Capture Flight Operations – Part 1 of 2: Mission Description, AR&C Exercises 1,2 and 3", AAS Spaceflight Mechanics Meeting 2008., Galveston TX. 2008.

3 Mulder. T, "Orbital Express Autonomous Rendezvous and Capture Flight Operations – Part 2 of 2: AR&C Exercises 4,5, and End of Life", AIAA/AAS Astrodynamics Specialist Conference, Honolulu, HI, Aug 2008.

4 Engineering Test Satellite VII (ETS-VII), http://robotics.jaxa.jp/project/ets7-HP/ets7_e/rvd/rvd_index_e.html#FP-1, accessed June 2009.

5 XSS-11 Mission Fact Sheet, Secure World Foundation, http://www.secureworldfoundation.org/siteadmin/images/files/file_356.pdf accessed 3 Jan 2009.

6 Vandenkerckhove, Jean., "Tankersat - Refueling satellites in Geosynchronous Orbit", AIAA Aeronautics and Astronautics 1982.

7 King, D., "On Demand Satellite Refueling", 8th Responsive Space Conference RS8-2010-6001, Los Angeles, CA.

8 Vivisat Web Site, www.vivisat.com.

9 Vallado, D. Fundamentals of Astrodynamics and Applications, 3rd Edition, Kluwer Academic Publishers , El Segundo California, 2001.

10 Ackermann, M., "Blind Search for Microsatellites in LEO: Optical Signatures and Search Strategies", AMOS Technical Conference 2005, Maui, HI.

11 Hall, D. et al. "Separating Attitude and Shape Effects for Non-resolved Objects", AMOS Technical Conference 2007, Maui HI.